ACS Biomaterials SCIENCE & ENGINEERING

pubs.acs.org/journal/abseba

Article

Promoting and Orienting Axon Extension Using Scaffold-Free Dental Pulp Stem Cell Sheets

Michelle D. Drewry, Matthew T. Dailey, Kristi Rothermund, Charles Backman, Kris N. Dahl, and Fatima N. Syed-Picard*

Cite This: *ACS Biomater. Sci. Eng.* 2022, 8, 814–825

Read Online

ACCESS | Metrics & More | Article Recommendations | Supporting Information

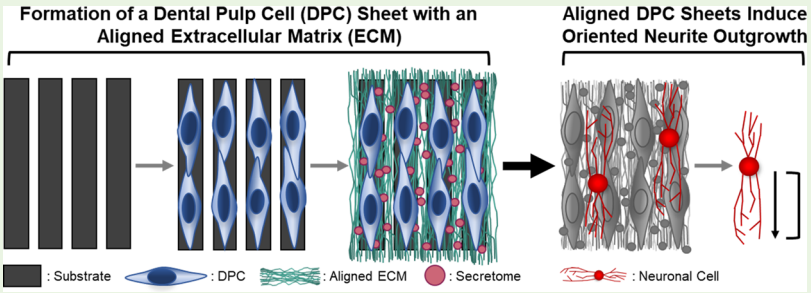

ABSTRACT: Current treatments of facial nerve injury result in poor functional outcomes due to slow and inefficient axon regeneration and aberrant reinnervation. To address these clinical challenges, bioactive scaffold-free cell sheets were engineered using neurotrophic dental pulp stem/progenitor cells (DPCs) and their aligned extracellular matrix (ECM). DPCs endogenously supply high levels of neurotrophic factors (NTFs), growth factors capable of stimulating axonal regeneration, and an aligned ECM provides guidance cues to direct axon extension. Human DPCs were grown on a substrate comprising parallel microgrooves, inducing the cells to align and deposit a linearly aligned, collagenous ECM. The resulting cell sheets were robust and could be easily removed from the underlying substrate. DPC sheets produced NTFs at levels previously shown capable of promoting axon regeneration, and, moreover, inducing DPC alignment increased the expression of select NTFs relative to unaligned controls. Furthermore, the aligned DPC sheets were able to stimulate functional neuritogenic effects in neuron-like cells *in vitro*. Neuronally differentiated neuroblastoma SH-SY5Y cells produced neurites that were significantly more oriented and less branched when cultured on aligned cell sheets relative to unaligned sheets. These data demonstrate that the linearly aligned DPC sheets can biomechanically support axon regeneration and improve axonal guidance which, when applied to a facial nerve injury, will result in more accurate reinnervation. The aligned DPC sheets generated here could be used in combination with commercially available nerve conduits to enhance their bioactivity or be formed into stand-alone scaffold-free nerve conduits capable of facilitating improved facial nerve recovery.

KEYWORDS: *scaffold-free, tissue engineering, peripheral nerve, facial nerve, dental pulp stem cells, regeneration*

INTRODUCTION

Facial nerve injuries, often caused by trauma, tumor ablation, or iatrogenic surgery, severely impact patients' quality of life, causing motor function impairment, which leads to facial paralysis and disfigurement. Twenty million Americans suffer from nerve injuries a year, and facial paralysis has an annual incidence of 11−40 cases per 100 000 with 127 000 new cases diagnosed annually in the United States.[1−4] The most severe peripheral nerve injuries are characterized by substantial loss of the nerve tissue. The current gold standard treatment for such segmental nerve injuries larger than 1 cm involves bridging the proximal and distal ends of the nerve with an autograft tissue. However, harvesting an autograft tissue is an invasive procedure, and it requires sacrificing a functional sensory nerve causing sensory loss at the donor site.[5,6] Even with treatment, regeneration is slow, extending up to 18 months, and full functional recovery is not achieved, resulting in asymmetric smile, oral incompetence, or lagophthalmos with potential for corneal injury.[7−9] In addition, due to the structure of their microanatomy, facial nerves are highly susceptible to synkinesis, in which the voluntary movement of one muscle leads to the involuntary movement of another muscle such as involuntary squinting of the eye as a patient attempts to smile.[9,10] Synkinesis is a result of axonal misdirection where

Received: December 2, 2021
Accepted: December 14, 2021
Published: January 4, 2022

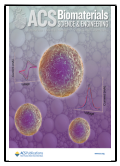

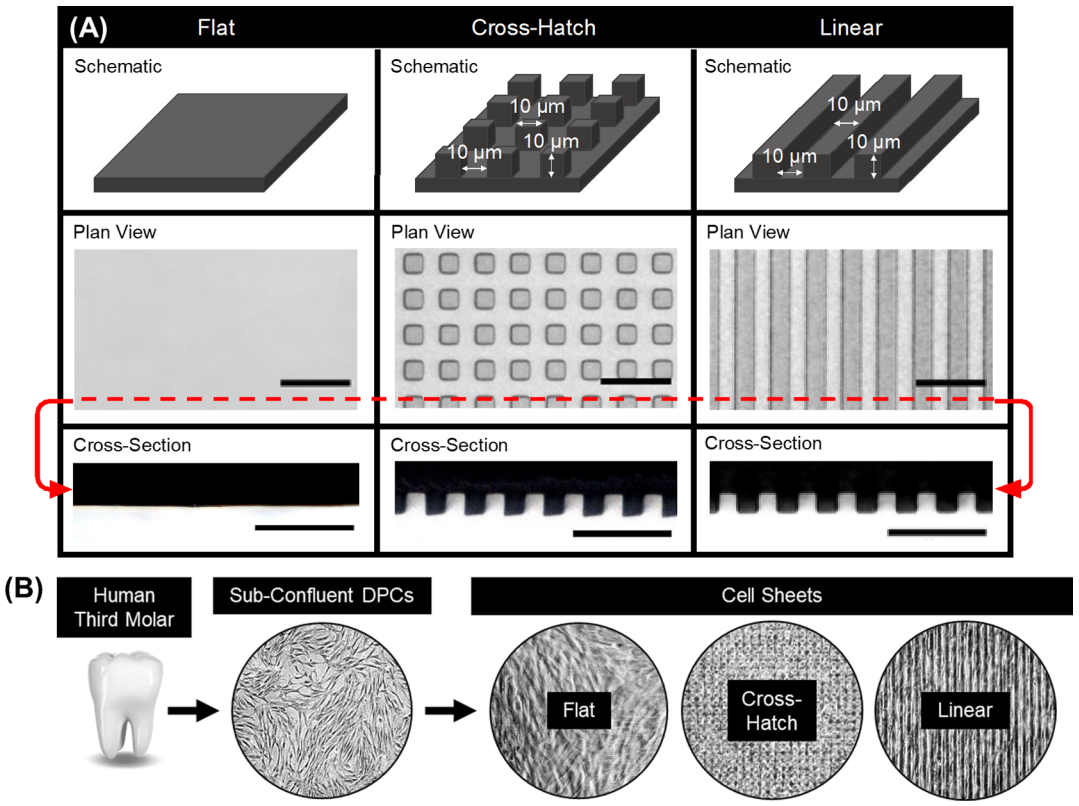

Figure 1. Overview of the substrate topography used to form DPC sheets. (A) Schematics of the substrates used to culture the cell sheets with representative plan view and cross-sectional bright-field images of the formed PDMS substrates. (B) Schematic of cell sheet formation, depicting the isolation of the cells from human third molars to form cell sheets on various substrates. Scale bars: (A) plan view = 40 μm, cross section = 50 μm.

regenerating axons branch and extend in aberrant directions, thus innervating incorrect postsynaptic targets. Correspondingly, axonal misdirection causes a reduced axonal density at the correct end organ, which contributes to reduced functional recovery. To bypass the challenges associated with the current standard of care, a significant amount of research has been directed toward engineering conduits to bridge segmental nerve injuries and provide (1) trophic cues to enhance and accelerate axonal regeneration and (2) guidance cues to orient axon extension toward the correct end organ.[11]

Neurotrophic factors (NTFs), such as the brain-derived NTF (BDNF), glial cell-derived NTF (GDNF), and neurotrophin 3 (NT-3), are a class of growth factors capable of promoting axonal growth and repair. NTFs are secreted in the native nerve environment by Schwann cells, neural-crest-derived glial cells that support peripheral nerve maintenance and regeneration. Previous studies have shown that treating damaged nerves with NTFs accelerated axon regeneration and improved functional recovery in animal models.[12,13] However, standard NTF treatment methods, such as direct injections, lack the sustained release needed for a substantial therapeutic effect.[14] Research has been directed toward developing cellular therapies using Schwann cells to promote sustained NTF delivery, but Schwann cells are difficult to maintain and expand in culture, limiting their therapeutic potential. Alternatively, multiple adult stem/progenitor cell populations, including those identified in the dental pulp, have also been shown to endogenously express NTFs. The dental pulp is the soft, vascular, and innervated tissue located in the center of the tooth and contains a population of stem/progenitor cells. Similar to Schwann cells, dental pulp cells (DPCs) are embryonically derived from the neural crest and endogenously express high levels of NTFs. DPCs have been shown to naturally produce more NTFs than other mesenchymal stem cells,[14,15] likely because of their shared developmental origins with Schwann cells. Furthermore, the safety and efficacy of both allogenic and autologous DPC-based therapies have been supported by various clinical trials.[16−21] Because of their capacity to endogenously express NTFs and the ongoing work supporting their use for therapeutic applications in humans, DPCs pose a promising candidate for cell-based nerve therapies.

Incorporating neurotrophic DPCs into a nerve conduit could improve the functional recovery of facial nerve injuries. Traditional tissue engineering methods could be used to embed DPCs directly into a three-dimensional (3D) scaffold material to form a bioactive conduit. However, difficulties remain in homogeneously incorporating cells into scaffolds, and numerous properties of scaffold biomaterials strongly affect the cell behavior. Additionally, *in vivo* degradation of the scaffold material can elicit inflammation.[22] Scaffold-free tissue engineering is an alternative technique that promotes cells to generate and organize their endogenous extracellular matrix (ECM) into a 3D tissue. Cell sheets are a form of scaffold-free tissue-engineered products created by cells laying down ECM to form a robust layer of tissue that can be separated from the underlying substrate and easily handled. Clinical trials using cell sheets to treat cardiac, ophthalmic, and dental disorders provide evidence of their safe and effective therapeutic potential.[23−25] Moreover, our lab has recently shown that

https://doi.org/10.1021/acsbiomaterials.1c01517
ACS Biomater. Sci. Eng. 2022, 8, 814−825

DPCs can form scaffold-free cell sheets capable of acting as an NTF delivery system and enhancing regeneration when wrapped around injured facial nerves of rats.[26] This previous work highlights the therapeutic potential of using scaffold-free DPC sheets for improving nerve repair.

While DPC sheets can be used to augment axonal regeneration by providing a trophic support, they lack the directional cues needed to guide the extending axons toward the correct post-synaptic target. Previous studies have shown that scaffolds comprising aligned ECM-scaled nanofibers can be used to orient extending neurites,[27] illustrating the potential use of topographical cues to direct axon extension in damaged nerves. Cell sheets can be engineered to contain an aligned ECM by culturing the cells on substrates with parallel linear microgrooves.[28−39] Such an aligned cell sheet could be used to guide regenerating axons, thus reducing synkinesis and improving functional outcomes.

The aim of this study is to engineer DPC sheets that provide both the sustained delivery of NTFs to promote axon regeneration and guidance cues from an aligned ECM to direct axon extension for use as bioactive materials to enhance facial nerve regeneration. We have previously shown that we can engineer DPC sheets that produce sufficient NTFs to improve repair in a rat facial nerve crush injury. In the current study, we hypothesized that culturing DPCs on a substrate with linearly aligned, microscaled grooves will lead to the formation of a similarly neurotrophic cell sheet that now also comprises a linearly aligned ECM. To test this, we evaluated the cell and ECM organization of DPC sheets cultured on substrates with microscaled topographies. We further tested the effects of substrate topography on NTF gene and protein expression by DPCs. Finally, we characterized the functional effects of the DPC sheets on neuritogenesis in neuron-like cells *in vitro*. The formation of a bioactive material that enhances axon regeneration and effectively orients extension would bypass the challenges associated with the current standard of care for treating nerve injuries.

MATERIALS AND METHODS

Isolation of DPCs. DPCs were isolated using methods similar to those previously described.[26,40,41] The dental pulp was isolated from healthy adult human third molars, collected at the University of Pittsburgh, School of Dental Medicine, and stored in 1× phosphate-buffered saline (PBS; Gibco) with 1× penicillin and streptomycin (P/S; Gibco). Within 24 h of extraction, the teeth were cracked open to remove the pulp. The pulp tissue was minced and then enzymatically digested for 1 h at 37 °C in 3 mg/mL collagenase (EMD Millipore) and 4 mg/mL dispase (Worthington Biochemical). The digest was passed through a 70 μm cell strainer, and the isolated DPCs were plated at an initial cell density of 5000−10 000 cells/cm^2 and cultured in Dulbecco's modified Eagle's medium (DMEM; Gibco), 20% fetal bovine serum (FBS; Atlanta Biologicals), and 1× P/S. The DPCs were expanded and cryopreserved, and cells from passage 2−5 were used to engineer the DPC sheets.

Formation of DPC Sheets. To form the DPC sheets, DPCs were cultured on either flat substrates or substrates with microscaled topographies of either linear grooves or cross-hatch structures (Figure 1). The linear grooved substrates were comprised of an array of parallel grooves that are 10 μm wide, spaced 10 μm apart, and 10 μm deep, and the cross-hatch grooves were 10 μm wide and spaced 10 μm apart, oriented 90° relative to each other, and were 10 μm deep. These polymer substrates were formed by curing Sylgard 184 polydimethylsiloxane (PDMS) in molds with the negative features and then cut and fit flush in the wells of a 12-well plate. Flat substrates were formed by curing PDMS directly in the plastic wells. Prior to use, the PDMS substrates were coated with 3 μg/cm^2 laminin (Gibco) and UV-sterilized. DPCs were then plated on the laminin-coated PDMS at an initial density of ∼32 000 cells/cm^2 in a growth medium containing DMEM, 20% FBS, 1% P/S, 5 μg/mL L-ascorbic acid (Sigma-Aldrich), and 5 ng/mL fibroblast growth factor (PeproTech), similar to that described previously.[26] Given that DPCs have a diameter of approximately 15 μm,[42] it is expected that cells will only attach and grow on the top surface of the grooves or within the troughs and likely not on the sides of the grooves. The culture medium was changed every 2−3 days, and a robust cell sheet formed after approximately 2 weeks. Individual cell sheets were used for all experiments in this study. Phase contrast images of the cell sheets was captured using a Nikon ECLIPSE Ti microscope.

Characterization of Cell and ECM Alignment. Cell sheets were washed twice with PBS, fixed in 10% formalin, and then permeabilized using 0.1% Triton 1× (Sigma-Aldrich). Immunohistochemical staining was performed using a primary antibody against type I collagen (Abcam) and secondary antibody Alexa Fluor 488 anti-rabbit IgG (ThermoFisher). In addition, phalloidin 594 (Abcam) was used to stain actin filaments and DAPI (Sigma-Aldrich) to visualize nuclei. Images were captured as *z*-stacks with a step size of 5 μm using a Nikon ECLIPSE Ti, ZEISS Scope.A1 AXIO or Nikon TE 2000 microscopes, and *z*-projections were obtained using the FIJI (ImageJ) software and the Extended Depth of Field plugin.[43] The nuclear alignment of the cell sheets was determined by measuring the angle of the major nuclei axes relative to the angle of the substrate features. Therefore, an alignment angle of 0° indicates that the major axis of a nucleus is aligned in parallel with the substrate topography. For the cell sheets cultured on flat PDMS, an arbitrary substrate feature angle was used. FIJI (ImageJ) was also used to quantify the orientation of the actin filaments and collagen fibers. Component images were first converted to an 8-bit grayscale, and directionality was assessed via the Fourier components plugin. Briefly, the Fourier transform determines the preferred orientation of subgroups within each image and sorts them into bins represented as histograms. Angles were measured with respect to the vertical axis and then transformed based on the angle of the substrate features. For all alignment quantifications, angles ranged from −90 to 90° and were separated into 10° bins, normalizing the number of counts per bin to the total number of features counted. Biological replicates were obtained using cells isolated from separate patients to generate cell sheets (n = 3); these biological replicates were averaged, and the resulting histograms were created using RStudio and the ggplot2 package.[44,45]

Scanning Electron Microscopy. Cell sheets were fixed using 2.5% glutaraldehyde (Sigma-Aldrich), post-fixed with osmium tetroxide (Sigma-Aldrich) and dehydrated using a series of ethanol washes. Samples were then dried, mounted on a metal stub, and sputter-coated with gold. Images were taken using a JSM 6335F scanning electron microscope (Top Analytica) and processed using the ImageJ software.

Histological Analysis. DPC sheets were washed twice with PBS and fixed in 10% formalin. Then, the cell sheets were processed for standard paraffin embedding and sectioned at a 5 μm thickness. Sections were stained with hematoxylin and eosin (H&E), or immunohistochemical staining was performed using a primary antibody against type I collagen (Abcam) and secondary antibody Alexa Fluor 488 anti-rabbit IgG (ThermoFisher). DAPI staining was used to visualize nuclei. Images were captured using a Nikon ECLIPSE Ti, ZEISS Scope.A1 AXIO or Nikon TE 2000 microscopes and processed using the ImageJ software.

Quantification of Cell Number. To quantify the number of cells in the DPC sheets, the sheets were digested in trypsin−EDTA (Gibco) at 37 °C for 10−20 min. The cells were then counted using a standard hemocytometer and trypan blue.

Quantitative Real-Time Polymerase Chain Reaction. RNA was isolated from the DPCs using the QIAGEN QIAshredder and RNeasy Mini kits as per the manufacturer's instructions, and RNA concentration was measured using a NanoDrop instrument (Thermo Scientific). Quantitative real-time polymerase chain reaction (qPCR) was performed with a TaqMan RNA to C_t One Step Kit (Applied

https://doi.org/10.1021/acsbiomaterials.1c01517
ACS Biomater. Sci. Eng. 2022, 8, 814−825

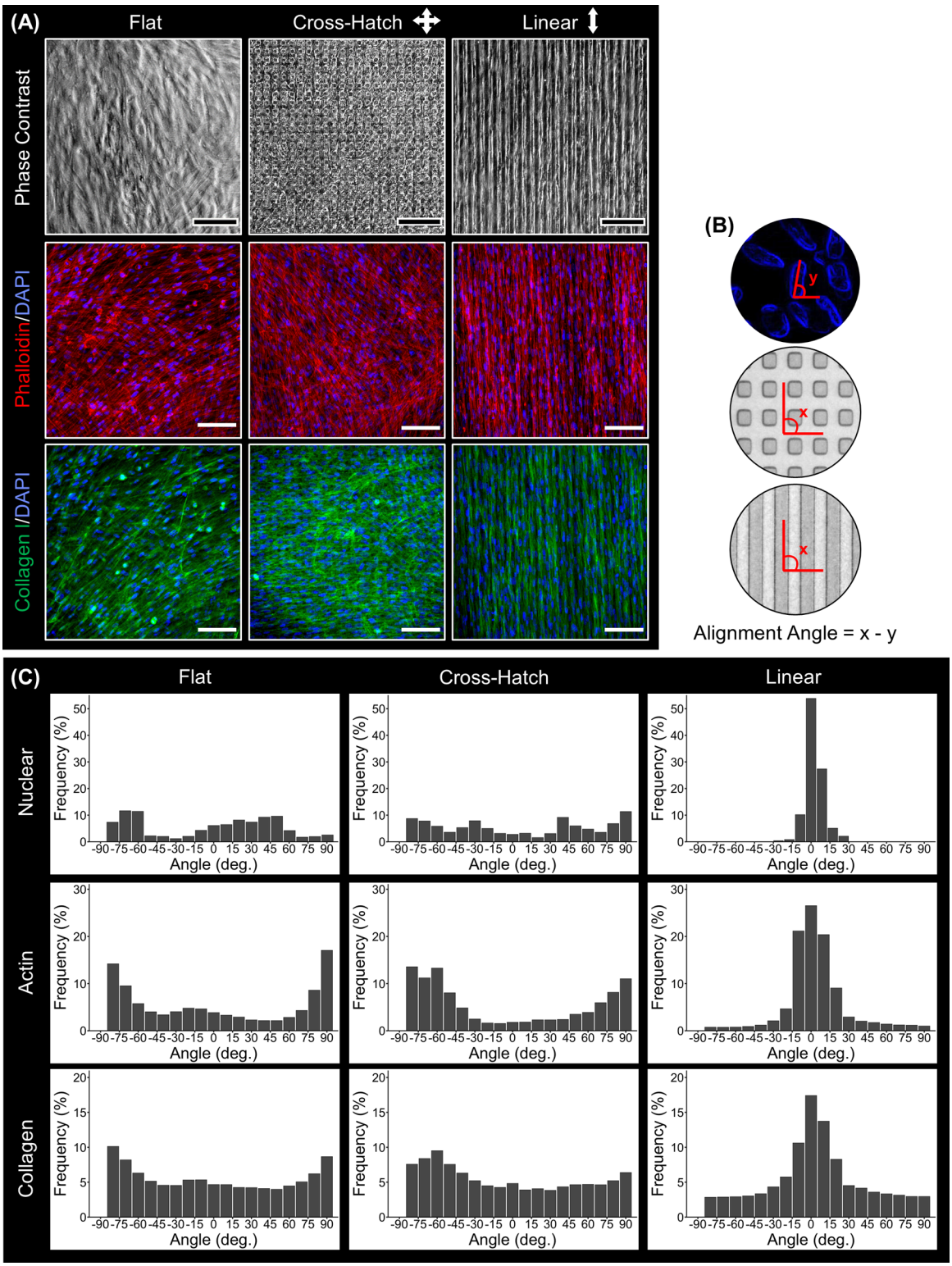

Figure 2. Characterization of cell and ECM alignment of DPC sheets cultured on flat or microgrooved substrates. (A) Phase contrast images, phalloidin staining (red), and collagen I (green) immunostaining of the DPC sheets show that the DPCs cultured on the linear microgrooves aligned in parallel with the linear microgrooves and generated an aligned ECM. (B) Schematic of the alignment quantification method. (C) Nuclear, actin cytoskeleton, and collagen I alignment were quantified for the cell sheets cultured on different topographies, validating that these features were linearly oriented on the linear but not on the flat or cross-hatch substrates. Scale bar: (A) 100 μm.

Biosystems) using primers of human BDNF, GDNF, NT-3, and housekeeping gene GAPDH (TaqMan Gene Expression Assays, Applied Biosystems). Relative gene expression was calculated using the $2^{-\Delta\Delta Ct}$ method, comparing the expression from DPCs cultured on substrates with microtopography to that of DPCs cultured on flat substrates.

Enzyme-Linked Immunosorbent Assay. Upon cell sheet formation, the culture medium was replaced with 0.5 mL for the NT-3 detection or 1 mL of the fresh culture medium for BDNF and

https://doi.org/10.1021/acsbiomaterials.1c01517
ACS Biomater. Sci. Eng. 2022, 8, 814−825

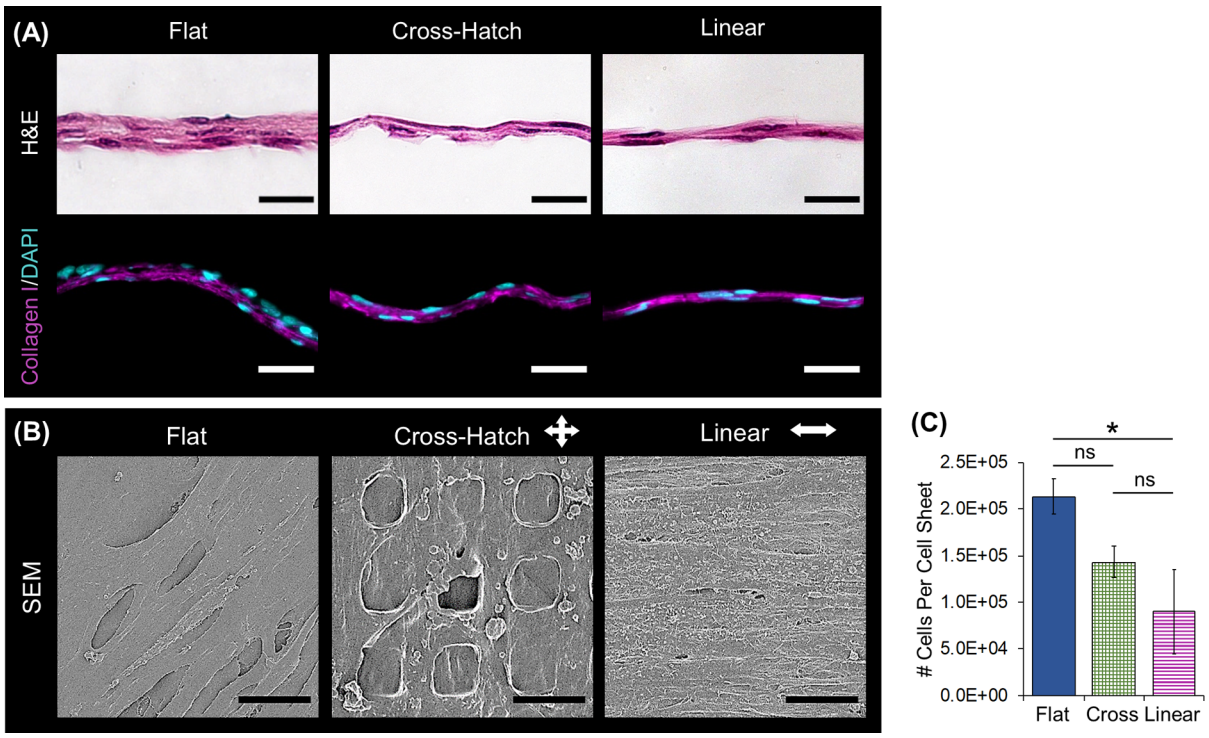

Figure 3. Structural characterization of the DPC sheets. (A) H&E staining illustrates that sheets cultured on all topographies were solid and cellular and those formed on the microtopographies were less thick than those cultured on the flat substrate. Immunostaining verifies that the DPC sheet ECM comprises type I collagen (magenta); nuclei were stained with DAPI (blue). (B) SEM further confirmed that the cell sheets contained a continuous matrix and that the sheets aligned their matrix when linear topographies. (C) Cell sheets cultured on the flat substrate contained more cells than those cultured on microtopographies (*: p-value < 0.05). Scale bars: (A) histology = 50 μm; (B) SEM = 15 μm.

GDNF analysis, and after 48 h, the conditioned medium (CM), containing the DPC secretome, was collected. The CM was centrifuged at 2000 rpm for 5 min to remove cellular debris, and the supernatant was collected and stored at −80 °C. Enzyme-linked immunosorbent assay (ELISA) kits for human BDNF (PicoKine ELISA Kit, Boster Biological Technology), GDNF (PicoKine ELISA Kit, Boster Biological Technology), and NT-3 (RayBiotech) were used to measure the protein concentration of the DPC sheet CM. The ELISAs were performed as per the manufacturer's instructions, and protein concentrations were extrapolated using standard curves generated using manufacturer-provided standards. Biological replicates (n = 4) were used to generate the figures. Statistical analyses were performed using RStudio,[44] and comparisons were made using the repeated one-way analysis of variance (ANOVA) and paired t-tests for the post-hoc tests.

Assessment of Neurite Extension *In Vitro*. SH-SY5Y (ATCC CRL2266) neuroblastoma cells were cultured in DMEM/F12 (Gibco), 10% FBS, and 1× P/S. After reaching 50% confluency, the cells were treated with a medium containing DMEM, 1% FBS, and 10 μM all-*trans*-retinoic acid (RA; Acros Organics) in order to differentiate the neuroblastoma cells into neuron-like cells, as done in previous studies.[26,46,47] Differentiation was validated by the presence of neurites and the expression of TUBB3, SYP, and MAP2 (Figure S1-Sn). Prior to co-culture with the DPC sheets, the neuronal cells were transfected with CellLight Tubulin-GFP (Invitrogen) as per the manufacturer's instructions. The labeled neuronal cells were plated on top of the cell sheet at a density of 3200 cells/cm^2.

After 3 days, the co-culture was washed with PBS, fixed in 10% formalin, and permeabilized using 0.1% Triton 1×. Immunohistochemical staining was performed using a primary antibody against type I collagen and secondary antibody Alexa Fluor 546 anti-rabbit IgG (ThermoFisher). DAPI was used to visualize nuclei. Images were captured as z-stacks with a step size of 0.5−5 μm using a Nikon ECLIPSE Ti, ZEISS Scope.A1 AXIO or Nikon TE 2000 microscopes. Deconvolutions were done using the NIS-Elements software (Nikon), and z-projections were performed using FIJI (ImageJ) and the Extended Depth of Field plugin.[43]

The alignment, net displacement, and branching of the SH-SY5Y neurites were quantified to determine the functional effects of the DPC sheets on the neuron-like cells. A neurite was defined as a projection greater than 2× the length of the soma. Neurite alignment was determined by measuring the angle of the neurites relative to substrate topography. The net displacement of the neurites was defined as the distance between the start of the neurite and the end of the neurite and was quantified using FIJI (ImageJ). The net displacement and alignment plots were made using RStudio and the ggplot2 package.[44,45] The number of branches per neurite were manually counted, and branching frequency was reported by normalizing to the total number of neurites evaluated. One-way ANOVA with Tukey's post-hoc tests was used to determine statistical differences (RStudio).[44] Over 250 neurites were analyzed for each experimental condition.

RESULTS

Formation of DPC Sheets with Aligned ECM. The goal of this study was to develop and characterize scaffold-free DPC sheets capable of enhancing facial nerve regeneration by providing neurotrophic cues to enhance axon regeneration and guidance cues to orient axon extension. DPC sheets were formed on a substrate with 10 μm linear microgrooves to induce the cells to deposit a linearly oriented ECM. It is well established that microscaled topographies can affect cell orientation, morphology, and differentiation;[48] therefore, to specifically evaluate the effects of aligned microgrooved substrates on DPC behavior, DPC sheets were also formed on control flat substrates or substrates with cross-hatch microgrooves (Figure 1). These experimental groups were selected to first control for the effects of culturing DPCs on a

https://doi.org/10.1021/acsbiomaterials.1c01517
ACS Biomater. Sci. Eng. 2022, 8, 814−825

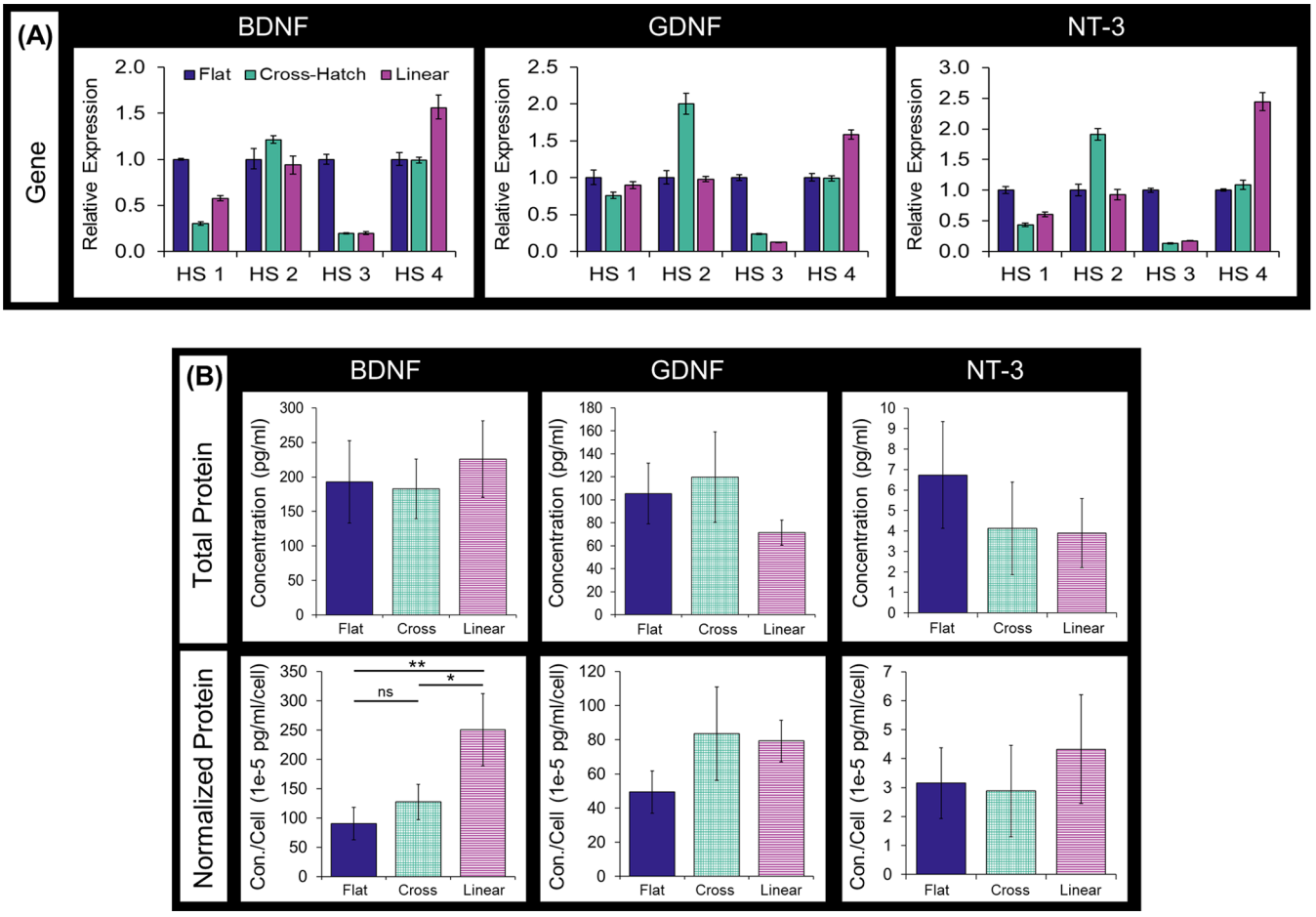

Figure 4. NTF expression by DPC sheets. (A) Analysis of the NTF mRNA expression using qPCR. Biological variability was evaluated by isolating mRNA from cell sheets formed using different human donor cells, denoting different human samples with HS. (B) Total BDNF, GDNF, and NT3 protein produced by DPC sheets, quantified by performing ELISA on the conditioned media of the sheets. Total protein was also normalized to average number of cells per cell sheet. The data represent an average of sheets formed using four different donor cells, and error bars indicate the standard deviation across biological replicates (*: p-value < 0.05, **: p-value < 0.005).

substrate with microscaled features (flat vs grooved substrates) and second to assess if the specific design of microscaled topography further alters cell behavior (linear vs cross-hatch microgrooves).

Phase contrast imaging shows that DPCs become confluent on all topographies (Figure 2A). Phalloidin staining (Figure 2A), which allowed visualization of the actin cytoskeleton, indicated that the DPCs aligned with the underlying linear grooves but maintained a disorganized arrangement on the flat or cross-hatch topography. Immunostaining (Figure 2A) showed that the ECM of the cell sheets contained type I collagen, and the collagenous ECM was linearly aligned in the DPC sheets formed on the linear microgrooves. To validate these observations, the nuclear, actin cytoskeleton, and collagen I alignments were quantified, comparing the angle of the feature of interest with the angle of the substrate, as demonstrated in Figure 2B. The resulting measurements are presented in Figure 2C. Evaluation of the DPC nuclear alignment showed that 92% of the nuclei were aligned (±10°) on the linear substrate compared to only 17 and 9.2% of the nuclei on the flat and cross-hatch substrates, respectively. As for the actin cytoskeleton, 68% of the filaments aligned (±10°) with the linear microgrooves, while only 12 and 5.2% of the actin filaments aligned on the flat and cross-hatch topographies, respectively. Finally, for the collagen alignment, 42, 15, and 13% of the collagen fibers aligned (±10°) in DPC sheets cultured linear, flat, and cross-hatch topographies, respectively. Overall, these data show that the linear microgrooved substrates induced DPCs to align and form a cell sheet with similarly aligned ECM.

Structural Characterization of the DPC Sheets. H&E staining of cross-sectional sections of the cell sheets indicated that on all substrate topographies, the DPCs formed solid tissues with multiple cell layers (Figure 3A). The sheets formed on the flat substrate were at least twice the thickness of those formed on the microtopographies. Furthermore, the cell sheets cultured on the flat substrate contained three layers of cells, while those on the microtopographies only contained two layers. Immunostaining on the histological sections validated the presence of type I collagen throughout the thickness of the cell sheet (Figure 3A). Scanning electron microscopy (SEM) showed that the cells cultured on the linear grooves formed a dense, aligned structure relative to those cultured on the other substrates (Figure 3B). In addition, the matrix of the cell sheets cultured on the cross-hatch substrate formed around the micropillars.

Quantification of the number of cells per cell sheet indicated that the cell sheets formed on the microtopographies tended to contain less cells than those formed on the flat substrate, with sheets on the flat substrate having significantly more cells than

https://doi.org/10.1021/acsbiomaterials.1c01517
ACS Biomater. Sci. Eng. 2022, 8, 814−825

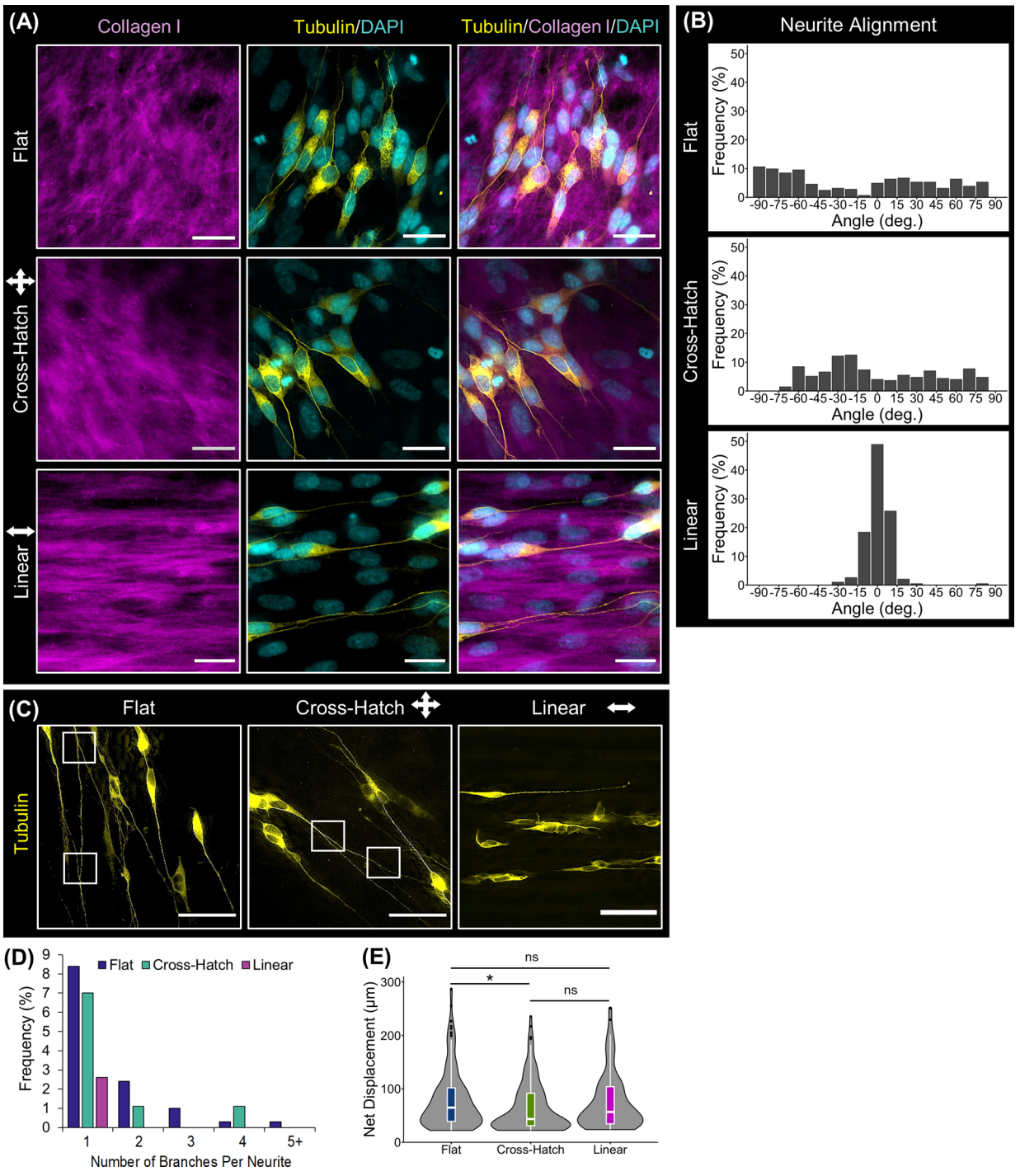

Figure 5. Functional effect of the DPC sheets on neuronal cells *in vitro*. (A) Neuronal cells with fluorescently labeled tubulin (yellow) were co-cultured on the DPC sheets. Immunostaining against collagen I (magenta) showed that neurites extended along the paths produced by the underlying ECM of the cell sheets. (B) Quantifying the alignment of the neurites validated that the majority of the neurites oriented linearly on the linearly organized cell sheets. (C) Global visualization of the neurites illustrated that more neurite branching was present on the disorganized cell sheets than the linearly aligned cell sheet, as denoted by the white boxes. (D) Quantifying the number of branches per neurite supported the observation that the neurites on the linearly organized cell sheets contained less branches than those on the disorganized cell sheets. (E) The length of the neurites was measured as their net displacement, showing that linear alignment of the neurites did not hinder their net displacement. The notches within the box plots indicate the median neurite net displacement, and black dots represent outliers (*: p-value < 0.05). Scale bars: (A) 100 and (B) 75 μm.

those on the linear substrate (p = 0.0149—Figure 3C). Cell viability was approximately 100% for all cell sheets, similar to the previous study.[26] While the linearly aligned cell sheets were thinner and contained less cells, they could still be easily removed from the substrate and handled similar to the flat cell sheets.

NTF Expression by DPC Sheets. The mRNA and protein expression of BDNF, GDNF, and NT-3 were measured to quantify the effect of substrate topography on DPC NTF

https://doi.org/10.1021/acsbiomaterials.1c01517
ACS Biomater. Sci. Eng. 2022, 8, 814−825

expression. Cell sheets formed using cells isolated from four healthy, independent donors were included to account for biological variability, and "HS" was used to denote these different human samples. Since there was variation in the NTF gene expression across patient cells, a generalized trend between substrate topography and NTF mRNA expression could not be detected across human samples (Figure 4A). The NTF protein expression by DPC sheets was determined by measuring the NTF concentration in DPC sheet-conditioned media, which contain the DPC secretome. NTF protein concentration was averaged across DPC sheets generated by cells from four separate patients (Figure 4B). Interestingly, substrate topography did not affect the total production of NTF proteins by the DPC sheets. We had found that substrate topography did affect the number of cells comprising the DPC sheet (Figure 3B). Normalizing total protein expression to the mean number of cells per sheet showed that the cells cultured on the microtopographies tended to produce higher levels of NTF per cell compared to those on the flat substrate, as seen in Figure 4B. This trend was statistically significant in the BDNF expression of the DPCs cultured on the linear compared to those formed on the flat (p-value = 0.00287) and cross-hatch (p-value = 0.0113) substrates. Therefore, while culturing DPCs on the microtopography may affect NTF production at the cell level, it did not affect the absolute amounts of NTF produced by DPC sheets due to differences in the number of cells per sheet.

Functional Effect of DPC Sheets on Neuronal Cells *In Vitro*. The functional effect of the DPC sheets on neuronal cells was evaluated by characterizing the ability of DPC sheets to induce neurite formation and direct the neurite extension of neuronally pre-differentiated SH-SY5Y cells. As seen in Figure 5A, the DPC sheets were able to induce neurite outgrowth, and these neurites appeared to align with the underlying DPC sheet ECM. Specifically, SH-SY5Y neurites extended linearly along the aligned collagenous ECM of the DPC sheets formed on the linear microgrooved topography. Quantification of neurite alignment showed that 93.2% of the neurites aligned linearly (±10°) on the linear cell sheets, whereas only 12.1 and 15.1% were aligned on the cell sheets formed on the flat and cross-hatch topographies, respectively (Figure 5B). These results verified that DPC sheets can promote neurite formation and orient extension.

When visualizing the neurites at a lower magnification, it was evident that the neurites on the linearly organized DPC sheets contained less branches than those on the disorganized sheets (Figure 5C). Quantifying this observation, only 2.6% of SH-SY5Y cells cultured in linearly aligned DPC sheets contained branches and, at most, one branch point was detected per neurite. However, 12.4 and 9.2% of neurites contained branches when the SH-SY5Y cells were cultured on the flat and cross-hatched sheets, respectively (Figure 5D), and these neurites contained up to 4 and 5 branch points. In addition, the neurites' net displacements were measured as a metric of the distance a neurite would grow toward its target organ (Figure 5E). While there was a significant decrease in the net displacement of the neurites on the cross-hatch relative to flat cell sheets (p = 0.0289), there was no statistically significant difference between those on the linear and flat cell sheets, suggesting that linear alignment of the neurites did not affect their net outgrowth. As for the neurites on the cross-hatch DPC sheets, they tended to grow in a less direct path compared to those on the other cell sheets, leading to the higher number of neurites with a short net displacement, as evident by the data distribution in Figure 5D. Therefore, linearly aligned DPC sheets were able to promote neuronal cells to exhibit oriented neurite extension while decreasing neurite branching and maintaining the neurite length.

DISCUSSION

In this study, we have engineered a bioactive material composed of neurotrophic DPCs and their endogenous, aligned ECM that is capable of promoting axon regeneration and orienting axon extension. While previous studies have separately demonstrated the efficacy of DPCs and aligned ECM-scaled topographies on enhancing nerve repair,[27,49] this study has uniquely combined these important factors together in a scaffold-free structure. Using such scaffold-free cell sheets as a vehicle for stem cell delivery addresses some of the challenges associated with cellular therapies that employ direct cell injections, specifically by facilitating high cell retention at injury sites as evidenced by our previous work.[26] In addition, aligned DPC sheets provide guidance cues lacking with cell injection therapies. Although scaffold-based cell delivery systems could also provide structures to orient axon extension, the scaffold-free system developed here bypasses challenges of scaffold-based treatments, such as issues with inhomogeneous cell incorporation into the exogenous delivery material. Furthermore, containing only cells and their endogenous ECM, cell sheets offer a more natural alternative compared to scaffold-based approaches. Overall, aligned scaffold-free DPC sheets are capable of delivering neurotrophic stem/progenitor cells more effectively than similarly organized scaffold-based constructs while providing guidance cues that would be absent with direct injections and thus have the potential to better enhance nerve repair.

Linear microgrooved PDMS substrates induced DPCs to align and deposit a linearly aligned ECM. It is well established that microtopographies can influence cell orientation and ECM alignment, as reviewed previously.[50,51] Specifically, substrate topographies are capable of affecting mesenchymal and neural stem cell alignment,[52−56] and our prior work showed that the specific microtopography used in this study could also orient corneal stromal stem cells.[57] Thus, this study validates that linear microgrooves can be used to align DPCs in a manner comparable to other stem cells and induce these aligned cells to lay down an aligned ECM and form a robust cell sheet. Similarly aligned cell sheets have been previously developed for use in repairing other organ systems,[29,31,35,36,39] but this is the first study to evaluate their potential effectiveness in treating peripheral nerve injuries.

DPC sheets formed on microscaled topographies contained less cells than those formed on the flat substrate. This phenomenon has previously been reported for multiple cell types including neural stem cells, embryonic stem cells, bone marrow stromal cells, and DPCs.[55,58−60] These prior works speculated that changes in cell phenotype or morphology in response to substrate topography caused a reduction in cell proliferation and correspondingly decreased resulting cell numbers. Furthermore, one study found that cells exhibited similar proliferation rates when cultured on linear and cross-hatch microgrooves,[54] indicating that microscaled topographies in general affect cell proliferation irrespective of topography design. The observed differences in the number of cells per sheet seen here likely contributed to the decreased overall thickness of the cell sheets cultured on the linear and

https://doi.org/10.1021/acsbiomaterials.1c01517
ACS Biomater. Sci. Eng. 2022, 8, 814−825

cross-hatch substrates compared to the flat. Despite these variations in cell number and sheet thickness, the cells in the linearly aligned sheets produced a dense and continuous matrix, forming a solid tissue that could be easily removed from the polymer substrate and handled. If needed, the linearly aligned cell sheets could be stacked to further increase the thickness and enhance the durability of these tissues. This would not only increase the thickness of the biomaterial but also increase its bioactivity through the addition of more neurotrophic DPCs.

Substrate patterning is known to provide mechanotransductive cues that affect the cell phenotype and differentiation.[48] Previous studies have demonstrated that the specific groove width (10 μm) of the substrates used in the current study was too wide to induce substantial adipogenic differentiation and too narrow for significant osteogenic or neural differentiation.[52,61] Here, we measured the effects of substrate topography on both the cell structure, including actin and nuclear alignment, and the neurotrophic activity of the DPC sheets. Substrate topography did not affect total NTF protein production by the DPC sheets. Furthermore, the levels of NTFs produced by the DPC sheets here are comparable to what we have previously shown to be sufficient to induce neuritogenesis *in vitro* and improve nerve repair *in vivo*.[26] Interestingly, the DPC sheets cultured on the topographies tended to comprise fewer cells than those formed on the flat substrates. Normalizing total NTF production to cell number showed that culturing DPCs on linearly grooved substrates induced increased BDNF production per cell. Although not statistically significant, a similar trend could also be seen for GDNF and NT3 expression; the presented data represented averaged biological replicates, which likely contributed to increased variance in the expression of these NTFs across samples. Prior to translating this therapy to clinical applications, future studies would be needed to determine factors that may contribute to this biological variability. Potentially, the prevalence of specific DPC subpopulations is correlated with increased NTF expression. If such a correlation exists, successful candidates could be screened on cell population-based criteria. Alternatively, DPC sheets comprising allogenic cells with known effective NTF expression could be utilized since both autologous and allogenic DPCs have been shown to be safe and efficacious in clinical studies.[16−21]

DPC sheets promoted and oriented neurite extension in SH-SY5Y neuron-like cells *in vitro*. The net displacement of neurite outgrowth was similar between DPC sheets comprising aligned or unorganized ECM, unlike previous studies which have found greater neurite extension on aligned nanofiber scaffolds compared to unaligned.[62−66] The scaffolds evaluated in these prior studies, nevertheless, did not contain stem/progenitor cells. Therefore, in the current study, neurite outgrowth may have been more driven by the neurotrophic support of the DPCs, which was similar between the different types of cell sheets, rather than topographical cues from an aligned substrate. We have previously shown that blocking the NTF receptors on SH-SY5Y cells reduced the neurotrophic effects of our DPC sheets, further highlighting that DPCs promote neurite elongation due to their NTF expression.[26] Thus, in the absence of DPCs, there would be a significant overall decrease in neurite growth. Additionally, neurite alignment was likely completely induced by the ECM of the cell sheet rather than any potential topographical cues from the underlying PDMS substrate. The DPC sheets ranged from 12 to 40 μm in thickness and would prevent any interactions between SH-SY5Y and the underlying PDMS. Furthermore, it has been previously demonstrated that wider topographies, similar in scale to the PDMS substrates used in this study, are less effective at inducing neurite alignment compared to narrower topographies, like that provided by the aligned ECM of the DPC sheets.[27]

When co-cultured with the DPC sheets, the neurites extended along with the underlying ECM of the cell sheets, corroborating previous work showing that neurites orient along ECM-scale nanofibers;[27] thus, DPC sheets comprising an aligned ECM were able to controllably orient the direction of neurite extension. Therefore, the aligned cell sheets generated here could be applied to an injured nerve to effectively minimize axon misdirection. Another contributor to aberrant reinnervation is axonal branching, which causes axons to innervate incorrect or multiple end organs. In this study, the linearly aligned DPC sheets not only guided neurite extension but also decreased neurite branching. Prior work has similarly reported that topographical guidance of axonal growth can reduce branching.[64,67] Potentially, direct guidance cues provide confined paths to orient axon extension, whereas, alternatively, indiscriminate cues supply multiple alternative routes causing axons to branch to simultaneously explore multiple aberrant directions.[67] Therefore, aligned DPC sheets have the potential to enhance functional recovery and minimize the occurrence of synkinesis following facial nerve repair by improving axonal guidance and diminishing axonal branching.

The aligned, DPC cell sheets generated here could serve as regenerative biomaterials for a variety of neural applications. For minor nerve injuries, such as compression or direct transection injuries, the sheets could be wrapped around the damaged nerve, protecting it from the surrounding cellular environment during healing while also providing support to enhance repair. For more severe injuries consisting of substantial tissue loss, the aligned DPC sheets could be formed into scaffold-free nerve conduits and be used to bridge segmental defects. Alternatively, these cell sheets could be combined with conduits already in use clinically to enhance bioactivity. Importantly, the use of aligned DPC sheets is not limited solely to facial nerves, and they could also be used in applications to repair other peripheral nerves or the spinal cord.

CONCLUSIONS

In this study, we have developed a bioactive material composed of DPCs and their endogenous aligned ECM. These DPC sheets are capable of enhancing facial nerve repair by providing both neurotrophic support, through the expression of NTFs, and guidance cues, through a linearly aligned ECM. This biomaterial is robust and can be used directly, to wrap injured nerves, or manipulated into a 3D conduit, to be used to bridge segmental nerve defects.

ASSOCIATED CONTENT

Supporting Information

The Supporting Information is available free of charge at https://pubs.acs.org/doi/10.1021/acsbiomaterials.1c01517.

Validation of the differentiation of neuroblastoma SH-SY5Y cells into neuron-like cells (PDF)

https://doi.org/10.1021/acsbiomaterials.1c01517
ACS Biomater. Sci. Eng. 2022, 8, 814−825

AUTHOR INFORMATION

Corresponding Author

Fatima N. Syed-Picard − *Department of Bioengineering, Swanson School of Engineering and Department of Oral Biology and Center for Craniofacial Regeneration, School of Dental Medicine, University of Pittsburgh, Pittsburgh, Pennsylvania 15213, United States; McGowan Institute for Regenerative Medicine, Pittsburgh, Pennsylvania 15219, United States*; Phone: 412-648-8824; Email: syedpicard@pitt.edu

Authors

Michelle D. Drewry − *Department of Bioengineering, Swanson School of Engineering, University of Pittsburgh, Pittsburgh, Pennsylvania 15213, United States;* orcid.org/0000-0001-5814-0223

Matthew T. Dailey − *Department of Oral and Maxillofacial Surgery, School of Dental Medicine, University of Pittsburgh, Pittsburgh, Pennsylvania 15213, United States*

Kristi Rothermund − *Department of Oral Biology and Center for Craniofacial Regeneration, School of Dental Medicine, University of Pittsburgh, Pittsburgh, Pennsylvania 15213, United States*

Charles Backman − *Department of Chemical Engineering, College of Engineering, Carnegie Mellon University, Pittsburgh, Pennsylvania 15213, United States*

Kris N. Dahl − *Department of Chemical Engineering, College of Engineering and Department of Biomedical Engineering, College of Engineering, Carnegie Mellon University, Pittsburgh, Pennsylvania 15213, United States; McGowan Institute for Regenerative Medicine, Pittsburgh, Pennsylvania 15219, United States; Forensics, Thornton Tomasetti, New York, New York 10271, United States*

Complete contact information is available at: https://pubs.acs.org/10.1021/acsbiomaterials.1c01517

Notes

The authors declare no competing financial interest.

ACKNOWLEDGMENTS

SEM was performed at the Center for Biological Imaging at the University of Pittsburgh with the help of Jonathan Franks. This research was supported by the National Institute of Dental and Craniofacial Research (R56 DE030881) to F.N.S. and the Osteo Science Foundation Resident Research Award to M.T.D. M.D.D. was supported by the Cellular Approaches to Tissue Engineering and Regeneration T32 training program (CATER; NIBIB, 5T32EB001026-14).

REFERENCES

(1) Gordin, E.; Lee, T. S.; Ducic, Y.; Arnaoutakis, D. Facial nerve trauma: evaluation and considerations in management. *Craniomaxillofacial Trauma Reconstr.* **2015**, *8*, 1−13.

(2) Guntinas-Lichius, O.; Hundeshagen, G.; Paling, T.; Angelov, D. N. Impact of different types of facial nerve reconstruction on the recovery of motor function: an experimental study in adult rats. *Neurosurgery* **2007**, *61*, 1276−1285.

(3) de Souza Lucena, E. E.; Guzen, F. P.; Lopes de Paiva Cavalcanti, J. R.; Galvão Barboza, C. A.; do Nascimento, E. S.; Cavalcante, J. d. S. Experimental considerations concerning the use of stem cells and tissue engineering for facial nerve regeneration: a systematic review. *J. Oral Maxillofac. Surg.* **2014**, *72*, 1001−1012.

(4) Bleicher, J. N.; Hamiel, S.; Gengler, J. S.; Antimarino, J. A Survey of Facial Paralysis: Etiology and Incidence. *Ear Nose Throat J.* **1996**, *75*, 355−358.

(5) Busuttil, F.; Rahim, A. A.; Phillips, J. B. Combining Gene and Stem Cell Therapy for Peripheral Nerve Tissue Engineering. *Stem Cells Dev.* **2017**, *26*, 231−238.

(6) Humphrey, C.; Kriet, J. Nerve repair and cable grafting for facial paralysis. *Facial Plast. Surg.* **2008**, *24*, 170−176.

(7) Flood, L. M. Facial Nerve Disorders and Diseases: Diagnosis and Management. *J. Laryngol. Otol.* **2016**, *130*, 507−508.

(8) Lindsay, R. W.; Heaton, J. T.; Edwards, C.; Smitson, C.; Hadlock, T. A. Nimodipine and acceleration of functional recovery of the facial nerve after crush injury. *Arch. Facial Plast. Surg.* **2010**, *12*, 49−52.

(9) Crumley, R. L. Mechanisms of Synkinesis. *Laryngoscope* **1979**, *89*, 1847−1854.

(10) Hadlock, T. A.; Kowaleski, J.; Lo, D.; Mackinnon, S. E.; Heaton, J. T. Rodent facial nerve recovery after selected lesions and repair techniques. *Plast. Reconstr. Surg.* **2010**, *125*, 99−109.

(11) López-Cebral, R.; Silva-Correia, J.; Reis, R. L.; Silva, T. H.; Oliveira, J. M. Peripheral Nerve Injury: Current Challenges, Conventional Treatment Approaches, and New Trends in Biomaterials-Based Regenerative Strategies. *ACS Biomater. Sci. Eng.* **2017**, *3*, 3098−3122.

(12) Gordon, T. The role of neurotrophic factors in nerve regeneration. *Neurosurg. Focus* **2009**, *26*, No. E3.

(13) Gordon, T.; Borschel, G. H. The use of the rat as a model for studying peripheral nerve regeneration and sprouting after complete and partial nerve injuries. *Exp. Neurol.* **2017**, *287*, 331−347.

(14) Mead, B.; Logan, A.; Berry, M.; Leadbeater, W.; Scheven, B. A. Intravitreally transplanted dental pulp stem cells promote neuroprotection and axon regeneration of retinal ganglion cells after optic nerve injury. *Invest. Ophthalmol. Visual Sci.* **2013**, *54*, 7544−7556.

(15) Mead, B.; Logan, A.; Berry, M.; Leadbeater, W.; Scheven, B. A. Paracrine-mediated neuroprotection and neuritogenesis of axotomised retinal ganglion cells by human dental pulp stem cells: comparison with human bone marrow and adipose-derived mesenchymal stem cells. *PLoS One* **2014**, *9*, No. e109305.

(16) Yamada, Y.; Nakamura-Yamada, S.; Kusano, K.; Baba, S. Clinical Potential and Current Progress of Dental Pulp Stem Cells for Various Systemic Diseases in Regenerative Medicine: A Concise Review. *Int. J. Mol. Sci.* **2019**, *20*, 1132.

(17) Collart-Dutilleul, P. Y.; Chaubron, F.; De Vos, J.; Cuisinier, F. J. Allogenic banking of dental pulp stem cells for innovative therapeutics. *World J. Stem Cells* **2015**, *7*, 1010−1021.

(18) d'Aquino, R.; De Rosa, A.; Lanza, V.; Tirino, V.; Laino, L.; Graziano, A.; Desiderio, V.; Laino, G.; Papaccio, G. Human mandible bone defect repair by the grafting of dental pulp stem/progenitor cells and collagen sponge biocomplexes. *Eur. Cells Mater.* **2009**, *18*, 75−83.

(19) Ferrarotti, F.; Romano, F.; Gamba, M. N.; Quirico, A.; Giraudi, M.; Audagna, M.; Aimetti, M. Human intrabony defect regeneration with micrografts containing dental pulp stem cells: A randomized controlled clinical trial. *J. Clin. Periodontol.* **2018**, *45*, 841−850.

(20) Nakashima, M.; Iohara, K.; Murakami, M.; Nakamura, H.; Sato, Y.; Ariji, Y.; Matsushita, K. Pulp regeneration by transplantation of dental pulp stem cells in pulpitis: a pilot clinical study. *Stem Cell Res. Ther.* **2017**, *8*, 61.

(21) Perry, B. C.; Zhou, D.; Wu, X.; Yang, F.-C.; Byers, M. A.; Chu, T.-M. G.; Hockema, J. J.; Woods, E. J.; Goebel, W. S. Collection, cryopreservation, and characterization of human dental pulp-derived mesenchymal stem cells for banking and clinical use. *Tissue Eng., Part C* **2008**, *14*, 149−156.

(22) Schmidt, C. E.; Leach, J. B. Neural tissue engineering: strategies for repair and regeneration. *Annu. Rev. Biomed. Eng.* **2003**, *5*, 293−347.

(23) Kim, Y. J.; Lee, H. J.; Ryu, J. S.; Kim, Y. H.; Jeon, S.; Oh, J. Y.; Choung, H. K.; Khwarg, S. I.; Wee, W. R.; Kim, M. K. Prospective Clinical Trial of Corneal Reconstruction With Biomaterial-Free

Cultured Oral Mucosal Epithelial Cell Sheets. *Cornea* **2018**, *37*, 76−83.
(24) Miyagawa, S.; Domae, K.; Yoshikawa, Y.; Fukushima, S.; Nakamura, T.; Saito, A.; Sakata, Y.; Hamada, S.; Toda, K.; Pak, K.; Takeuchi, M.; Sawa, Y. Phase I Clinical Trial of Autologous Stem Cell-Sheet Transplantation Therapy for Treating Cardiomyopathy. *J. Am. Heart Assoc.* **2017**, *6*, No. e003918.
(25) Iwata, T.; Yamato, M.; Washio, K.; Yoshida, T.; Tsumanuma, Y.; Yamada, A.; Onizuka, S.; Izumi, Y.; Ando, T.; Okano, T.; Ishikawa, I. Periodontal regeneration with autologous periodontal ligament-derived cell sheets - A safety and efficacy study in ten patients. *Regener. Ther.* **2018**, *9*, 38−44.
(26) Ahmed, M. N.; Shi, D.; Dailey, M. T.; Rothermund, K.; Drewry, M. D.; Calabrese, T. C.; Cui, X. T.; Syed-Picard, F. N. Dental Pulp Cell Sheets Enhance Facial Nerve Regeneration via Local Neurotrophic Factor Delivery. *Tissue Eng., Part A* **2020**, *27*, 1128−1139.
(27) Simitzi, C.; Ranella, A.; Stratakis, E. Controlling the morphology and outgrowth of nerve and neuroglial cells: The effect of surface topography. *Acta Biomater.* **2017**, *51*, 21−52.
(28) Allen, A. C. B.; Barone, E.; Crosby, C. O. K.; Suggs, L. J.; Zoldan, J. Electrospun poly(N-isopropyl acrylamide)/poly-(caprolactone) fibers for the generation of anisotropic cell sheets. *Biomater. Sci.* **2017**, *5*, 1661−1669.
(29) Backman, D. E.; LeSavage, B. L.; Shah, S. B.; Wong, J. Y. A Robust Method to Generate Mechanically Anisotropic Vascular Smooth Muscle Cell Sheets for Vascular Tissue Engineering. *Macromol. Biosci.* **2017**, *17*, 1600434.
(30) Beachley, V.; Hepfer, R.; Katsanevakis, E.; Zhang, N.; Wen, X. Precisely Assembled Nanofiber Arrays as a Platform to Engineer Aligned Cell Sheets for Biofabrication. *Bioengineering* **2014**, *1*, 114−133.
(31) Chuah, Y. J.; Tan, J. R.; Wu, Y.; Lim, C. S.; Hee, H. T.; Kang, Y.; Wang, D.-A. Scaffold-Free tissue engineering with aligned bone marrow stromal cell sheets to recapitulate the microstructural and biochemical composition of annulus fibrosus. *Acta Biomater.* **2020**, *107*, 129−137.
(32) Dang, J. M.; Leong, K. W. Myogenic Induction of Aligned Mesenchymal Stem Cell Sheets by Culture on Thermally Responsive Electrospun Nanofibers. *Adv. Mater.* **2007**, *19*, 2775−2779.
(33) Fu, S.-W.; Chien, H.-W.; Tsai, W.-B. Fabrication of poly(N-isopropylacrylamide) films containing submicrometer grooves for constructing aligned cell sheets. *Langmuir* **2013**, *29*, 14351−14355.
(34) Fujie, T.; Shi, X.; Ostrovidov, S.; Liang, X.; Nakajima, K.; Chen, Y.; Wu, H.; Khademhosseini, A. Spatial coordination of cell orientation directed by nanoribbon sheets. *Biomaterials* **2015**, *53*, 86−94.
(35) Isenberg, B. C.; Backman, D. E.; Kinahan, M. E.; Jesudason, R.; Suki, B.; Stone, P. J.; Davis, E. C.; Wong, J. Y. Micropatterned cell sheets with defined cell and extracellular matrix orientation exhibit anisotropic mechanical properties. *J. Biomech.* **2012**, *45*, 756−761.
(36) Lim, J.; Jun, I.; Lee, Y. B.; Kim, E. M.; Shin, D.; Jeon, H.; Park, H.; Shin, H. Fabrication of cell sheets with anisotropically aligned myotubes using thermally expandable micropatterned hydrogels. *Macromol. Res.* **2016**, *24*, 562−572.
(37) Takahashi, H.; Nakayama, M.; Shimizu, T.; Yamato, M.; Okano, T. Anisotropic cell sheets for constructing three-dimensional tissue with well-organized cell orientation. *Biomaterials* **2011**, *32*, 8830−8838.
(38) Takahashi, H.; Shimizu, T.; Nakayama, M.; Yamato, M.; Okano, T. The use of anisotropic cell sheets to control orientation during the self-organization of 3D muscle tissue. *Biomaterials* **2013**, *34*, 7372−7380.
(39) Williams, C.; Xie, A. W.; Yamato, M.; Okano, T.; Wong, J. Y. Stacking of aligned cell sheets for layer-by-layer control of complex tissue structure. *Biomaterials* **2011**, *32*, 5625−5632.
(40) Basu, A.; Rothermund, K.; Ahmed, M. N.; Syed-Picard, F. N. Self-Assembly of an Organized Cementum-Periodontal Ligament-Like Complex Using Scaffold-Free Tissue Engineering. *Front. Physiol.* **2019**, *10*, 422.
(41) Syed-Picard, F. N.; Ray, H. L., Jr.; Kumta, P. N.; Sfeir, C. Scaffoldless tissue-engineered dental pulp cell constructs for endodontic therapy. *J. Dent. Res.* **2014**, *93*, 250−255.
(42) Suchanek, J.; Soukup, T.; Visek, B.; Ivancakova, R.; Kucerova, L.; Mokry, J. Dental pulp stem cells and their characterization. *Biomed. Pap. Med. Fac. Palacky Univ. Olomouc Czech Repub.* **2009**, *153*, 31−35.
(43) Forster, B.; Van De Ville, D.; Berent, J.; Sage, D.; Unser, M. Extended depth-of-focus for multi-channel microscopy images: A complex wavelet approach. *2004 2nd IEEE International Symposium on Biomedical Imaging: Macro to Nano (IEEE Cat No. 04EX821)*; IEEE, 2004, pp 660−663.
(44) Team, R. *RStudio: Integrated Development Environment for R, 1.4*; RStudio, PBC: Boston, MA, 2021.
(45) Wickham, H. *ggplot2: Elegant Graphics for Data Analysis*; Springer-Verlag: New York, 2016.
(46) Påhlman, S.; Ruusala, A. I.; Abrahamsson, L.; Mattsson, M. E.; Esscher, T. Retinoic acid-induced differentiation of cultured human neuroblastoma cells: a comparison with phorbolester-induced differentiation. *Cell Differ.* **1984**, *14*, 135−144.
(47) Gervois, P.; Wolfs, E.; Dillen, Y.; Hilkens, P.; Ratajczak, J.; Driesen, R. B.; Vangansewinkel, T.; Bronckaers, A.; Brône, B.; Struys, T.; Lambrichts, I. Paracrine Maturation and Migration of SH-SY5Y Cells by Dental Pulp Stem Cells. *J. Dent. Res.* **2017**, *96*, 654−662.
(48) Ding, S.; Kingshott, P.; Thissen, H.; Pera, M.; Wang, P.-Y. Modulation of human mesenchymal and pluripotent stem cell behavior using biophysical and biochemical cues: A review. *Biotechnol. Bioeng.* **2017**, *114*, 260−280.
(49) Luo, L.; He, Y.; Wang, X.; Key, B.; Lee, B. H.; Li, H.; Ye, Q. Potential Roles of Dental Pulp Stem Cells in Neural Regeneration and Repair. *Stem Cells Int.* **2018**, *2018*, 1731289.
(50) Mirbagheri, M.; Adibnia, V.; Hughes, B. R.; Waldman, S. D.; Banquy, X.; Hwang, D. K. Advanced cell culture platforms: a growing quest for emulating natural tissues. *Mater. Horiz.* **2019**, *6*, 45−71.
(51) Leclech, C.; Villard, C. Cellular and Subcellular Contact Guidance on Microfabricated Substrates. *Front. Bioeng. Biotechnol.* **2020**, *8*, 551505.
(52) Abagnale, G.; Steger, M.; Nguyen, V. H.; Hersch, N.; Sechi, A.; Joussen, S.; Denecke, B.; Merkel, R.; Hoffmann, B.; Dreser, A.; Schnakenberg, U.; Gillner, A.; Wagner, W. Surface topography enhances differentiation of mesenchymal stem cells towards osteogenic and adipogenic lineages. *Biomaterials* **2015**, *61*, 316−326.
(53) Gong, T.; Zhao, K.; Yang, G.; Li, J.; Chen, H.; Chen, Y.; Zhou, S. The control of mesenchymal stem cell differentiation using dynamically tunable surface microgrooves. *Adv. Healthcare Mater.* **2014**, *3*, 1608−1619.
(54) Li, Z.; Gong, Y.; Sun, S.; Du, Y.; Lü, D.; Liu, X.; Long, M. Differential regulation of stiffness, topography, and dimension of substrates in rat mesenchymal stem cells. *Biomaterials* **2013**, *34*, 7616−7625.
(55) Qi, L.; Li, N.; Huang, R.; Song, Q.; Wang, L.; Zhang, Q.; Su, R.; Kong, T.; Tang, M.; Cheng, G. The effects of topographical patterns and sizes on neural stem cell behavior. *PLoS One* **2013**, *8*, No. e59022.
(56) Zahor, D.; Radko, A.; Vago, R.; Gheber, L. A. Organization of mesenchymal stem cells is controlled by micropatterned silicon substrates. *Mater. Sci. Eng., C* **2007**, *27*, 117−121.
(57) Syed-Picard, F. N.; Du, Y.; Hertsenberg, A. J.; Palchesko, R.; Funderburgh, M. L.; Feinberg, A. W.; Funderburgh, J. L. Scaffold-free tissue engineering of functional corneal stromal tissue. *J. Tissue Eng. Regener. Med.* **2018**, *12*, 59−69.
(58) Gerecht, S.; Bettinger, C. J.; Zhang, Z.; Borenstein, J. T.; Vunjak-Novakovic, G.; Langer, R. The effect of actin disrupting agents on contact guidance of human embryonic stem cells. *Biomaterials* **2007**, *28*, 4068−4077.
(59) Kolind, K.; Kraft, D.; Bøggild, T.; Duch, M.; Lovmand, J.; Pedersen, F. S.; Bindslev, D. A.; Bünger, C. E.; Foss, M.; Besenbacher, F. Control of proliferation and osteogenic differentiation of human

dental-pulp-derived stem cells by distinct surface structures. *Acta Biomater.* **2014**, *10*, 641−650.
(60) McMurray, R. J.; Wann, A. K. T.; Thompson, C. L.; Connelly, J. T.; Knight, M. M. Surface topography regulates wnt signaling through control of primary cilia structure in mesenchymal stem cells. *Sci. Rep.* **2013**, *3*, 3545.
(61) Béduer, A.; Vieu, C.; Arnauduc, F.; Sol, J.-C.; Loubinoux, I.; Vaysse, L. Engineering of adult human neural stem cells differentiation through surface micropatterning. *Biomaterials* **2012**, *33*, 504−514.
(62) Berns, E. J.; Sur, S.; Pan, L.; Goldberger, J. E.; Suresh, S.; Zhang, S.; Kessler, J. A.; Stupp, S. I. Aligned neurite outgrowth and directed cell migration in self-assembled monodomain gels. *Biomaterials* **2014**, *35*, 185−195.
(63) Corey, J. M.; Lin, D. Y.; Mycek, K. B.; Chen, Q.; Samuel, S.; Feldman, E. L.; Martin, D. C. Aligned electrospun nanofibers specify the direction of dorsal root ganglia neurite growth. *J. Biomed. Mater. Res., Part A* **2007**, *83A*, 636−645.
(64) Patel, S.; Kurpinski, K.; Quigley, R.; Gao, H.; Hsiao, B. S.; Poo, M.-M.; Li, S. Bioactive nanofibers: synergistic effects of nanotopography and chemical signaling on cell guidance. *Nano Lett.* **2007**, *7*, 2122−2128.
(65) Zhu, W.; Masood, F.; O'Brien, J.; Zhang, L. G. Highly aligned nanocomposite scaffolds by electrospinning and electrospraying for neural tissue regeneration. *Nanomedicine* **2015**, *11*, 693−704.
(66) Lanfer, B.; Hermann, A.; Kirsch, M.; Freudenberg, U.; Reuner, U.; Werner, C.; Storch, A. Directed growth of adult human white matter stem cell-derived neurons on aligned fibrillar collagen. *Tissue Eng., Part A* **2010**, *16*, 1103−1113.
(67) Omidinia-Anarkoli, A.; Ephraim, J. W.; Rimal, R.; De Laporte, L. Hierarchical fibrous guiding cues at different scales influence linear neurite extension. *Acta Biomater.* **2020**, *113*, 350−359.

https://doi.org/10.1021/acsbiomaterials.1c01517
ACS Biomater. Sci. Eng. 2022, 8, 814−825